

Contents lists available at ScienceDirect

Acta Biomaterialia

journal homepage: www.elsevier.com/locate/actbio



Full length article

Role of the microtubule network in the passive anisotropic viscoelasticity of right ventricle with pulmonary hypertension progression

Kristen LeBar^a, Wenqiang Liu^{b,c}, Jassia Pang^d, Adam J. Chicco^e, Zhijie Wang^{a,b,*}

- ^a Department of Mechanical Engineering, Colorado State University, Fort Collins, CO USA
- ^b School of Biomedical Engineering, Colorado State University, Fort Collins, CO USA
- ^c Stanford Cardiovascular Institute, Stanford University, Stanford, CA USA
- ^d Laboratory Animal Resources, Colorado State University, Fort Collins, CO USA
- ^c Department of Biomedical Sciences, Colorado State University, Fort Collins, CO USA

article info

Received 8 October 2023 Revised 28 December 2023 Accepted 17 January 2024 Available online xxx

Keywords. Myocardial mechanics Myofiber Constitutive modeling Colchicine

abstract

Cardiomyocytes are viscoelastic and contribute significantly to right ventricle (RV) mechanics. Microtubule, a cytoskeletal protein, has been shown to regulate cardiomyocyte viscoelasticity. Additionally, hypertrophied cardiomyocytes from failing myocardium have increased microtubules and cell stiffness. How the microtubules contribute to the tissue-level viscoelastic behavior in RV failure remains unknown. Our aim was to investigate the role of the microtubules in the passive anisotropic viscoelasticity of the RV free wall (RVFW) during pulmonary hypertension (PH) progression. Equibiaxial stress relaxation tests were conducted in the RVFW from healthy and PH rats under early (6%) and end (15%) diastolic strains, and at sub- (1Hz) and physiological (5Hz) stretch-rates. The RVFW viscoelasticity was also measured before and after the depolymerization of microtubules at 5Hz. In intact tissues, PH increased RV viscosity and elasticity at both stretch rates and strain levels, and the increase was stronger in the circumferential than longitudinal direction. At 6% of strain, the removal of microtubules reduced elasticity, viscosity, and the ratio of viscosity to elasticity in both directions and for both healthy and diseased RVs. However, at 15% of strain, the effect of microtubules was different between groups - both viscosity and elasticity were reduced in healthy RVs, but in the diseased RVs only the circumferential viscosity and the ratio of viscosity to elasticity were reduced. These data suggest that, at a large strain with collagen recruitment, microtubules play more significant roles in healthy RV tissue elasticity and diseased RV tissue viscosity. Our findings suggest cardiomyocyte cytoskeletons are critical to RV passive viscoelasticity under pressure overload.

Statement of Significance

This study investigated the impact of microtubules on the passive anisotropic viscoelasticity of the right ventricular (RV) free wall at healthy and pressure-overloaded states. We originally found that the microtubules contribute significantly to healthy and diseased RV viscoelasticity in both (longitudinal and circumferential) directions at early diastolic strains. At end diastolic strains (with the engagement of collagen fibers), microtubules contribute more to the tissue elasticity of healthy RVs and tissue viscosity of diseased RVs. Our findings reveal the critical role of microtubules in the anisotropic viscoelasticity of the RV tissue, and the altered contribution from healthy to diseased state suggests that therapies targeting microtubules may have potentials for RV failure patients.

Published by Elsevier Ltd on behalf of Acta Materialia Inc.

1. Introduction

Heart failure (HF) is the leading cause of death in the US and worldwide [1], and ventricular dysfunction is a main contributor to HF. Specifically, right ventricular (RV) failure contributes

E-mail address: Zhijie.wang@colostate.edu (Z. Wang).

https://doi.org/10.1016/j.actbio.2024.01.023 1742-7061/Published by Elsevier Ltd on behalf of Acta Materialia Inc.

Please cite this article as: K. LeBar, W. Liu, J. Pang et al., Role of the microtubule network in the passive anisotropic viscoelasticity of right ventricle with pulmonary hypertension progression, Acta Biomaterialia, https://doi.org/10.1016/j.actbio.2024.01.023

^{*} Corresponding author.

significantly to the mortality and morbidity of various cardiovascular diseases, such as congenital heart disease, left ventricular failure with preserved ejection fraction (HFpEF), and pulmonary hypertension (PH). There has still, though, been a lack of treatment for such patients, due largely to a lack of understanding of the pathology and physiology of RV failure. It is accepted that the mechanical behavior of the organ largely impacts its function [2–5]. A prior rodent study found a correlation between the passive stiffness of the RV and end diastolic volume [3], and our own ovine study showed that RV elasticity is positively correlated with geometry and hemodynamic properties [2]. While such studies suggest a key role of the organ elastic behavior in clinical parameters, the RV is viscoelastic. This indicates that the tissue exhibits both elastic and viscous resistance in response to deformation.

There has been increasing evidence of myocardial tissue viscoelasticity in both the left and right ventricle (LV, RV), including those from our group [6-10]. The RV free wall (RVFW) is comprised of myofibers, collagen, vasculature, extracellular matrix (ECM) components, as well as interstitial fluids. These components all exhibit viscoelastic properties. Moreover, due to the complex organizations with intra- and extracellular bonds, alignment, layered structures, and uneven density/distribution of these components in physiology and pathology conditions, the anisotropic mechanical behavior is evident. Cardiomyocytes (CM) or papillary muscles are known to demonstrate viscoelastic behavior [11-16], and CM are key determinants of the contractile function of the myocardium, which is directly related to the viscoelasticity of the cell [13,17,18]. A recent study of isolated healthy CM showed that the depolymerization via colchicine of the microtubule (MT), a cytoskeletal structure of the cell, reduces the cell's viscoelasticity and strengthens the degree and velocity of shortening [19], suggesting a key role of the MT network in the mechanical behavior of the CM and its contractile function. Additionally, Caporizzo et al. treated isolated adult healthy CM from the LV with colchicine and observed a weakened cell viscosity and elasticity [13]. These studies, though, only obtained healthy cell behavior. In the hypertrophied myocardium, both MT density and myofiber viscoelasticity are increased [17,20]. Moreover, the treatment of colchicine on isolated adult CM from a failing LV still reduced the cell elasticity and viscosity [17]. While both stress relaxation and cyclic mechanical tests were conducted, the distinct role of the MT network on the failing RV mechanical behavior remains unknown.

Therefore, the aim of this study is to characterize the role of the MT network in RV passive anisotropic viscoelasticity during PH progression. We induced PH in adult rats and performed equibiaxial stress relaxation testing on the entire RVFW with and without the treatment of colchicine to depolymerize the MT network. Then the experimental data was fit using a quasilinear viscoelastic (QLV) constitutive model established previously to further delineate the effect of the MT network to RV relaxation strength with pressure overload. Our study revealed that 1) PH enhances RV elasticity and viscosity, and the increase was stronger in the circumferential than longitudinal directions; 2) the stretch rate, not strain level, differently affected the elasticity and viscosity of the healthy and diseased RVs; 3) at the early diastolic strain level, the removal of MT network reduced tissue elasticity, viscosity, and the ratio of viscosity to elasticity in both directions and for both healthy and diseased RVs; 4) at the end diastolic strain level, the removal of MT network reduced viscosity and elasticity in healthy RVs, but it only reduced the circumferential viscosity and the ratio of viscosity to elasticity in diseased RVs. The results from different strains suggest that the impact of MT on tissue viscoelasticity is different before and after collagen recruitment. To our knowledge, this is the first study to investigate the role of MT network in the viscoelastic behavior of hypertrophied myocardium. Our data has revealed a critical contribution of MT to the viscoelastic resistance of RV tissue at both healthy and diseased states. These findings deepen the understanding of cytoskeleton determinants of RV mechanics and may shed light on their contribution to the pathophysiology of RV failure

2. Materials and methods

2.1. Specimen preparation and disease model

All animal procedures were approved by the Colorado State University Institutional Animal Care and Use Committees (IACUC, protocol #1438). 6-week-old male Sprague-Dawley rats (n=6) were administered a subcutaneous injection (60mg/kg) of monocrotaline (MCT) to induce PH and housed in normal conditions for three weeks. We followed the identical disease model protocol as described previously, in which we observed overt PH [21]. Healthy age matched male animals served as control (CTL) (n=6). At 3 weeks post treatment, the animals were euthanized, and the heart was excised and placed in phosphate buffer solution (PBS) on ice.

2.2. Ex vivo equibiaxial mechanical testing

After harvest, the entire RVFW was dissected in cardioplegic solution (CPS) and fully submerged in 30mM 2,3-butanedione monoxime (BDM) solution at body temperature for 30 minutes prior to testing to remove the contractility of the myocardium. The tissue remained submerged in the solution for the remainder of the testing period. The tissue was then preloaded to approximately 0.05 N to specify the zero-stress configuration, and calipers were used to measure the dimensions of the square sample. The square shaped tissue sample ($\sim 10 \times 10 \text{ mm}^2$ in CTL group and $\sim 15 \times 15$ mm² in MCT group) was mounted on four vertical tines on the biaxial tester, and the outflow tract direction was defined as the longitudinal (L) direction. The tissue thickness was approximately 0.9~1.3 mm in these groups, and thus negligible shear deformation requirement is fulfilled in the biaxial planar test [22]. Four markers were placed on the center region of the surface in a square formation for strain analysis. 10-15 cycles of cyclic equibiaxial preconditioning were then conducted (at 1Hz and 20% maximal strain) to reach an equilibrium stress in the tissue (Supplemental Figure S1) [23] .

RV tissue then underwent equibiaxial stress relaxation to obtain the passive, biaxial viscoelastic behavior using an in-house biaxial tester [21,24]. In the displacement-controlled test, the RV was stretched to the global strains of 6% and 15%, which correspond to the early and late diastolic strains, respectively, to examine the viscoelastic behavior at small and large deformations [3,21]. For each strain level, the tissue was tested at two stretch (ramp) rates: 30%/s and 150%/s, which relate to a sub-physiological (1Hz) and physiological (5Hz) heart rate of the adult rat, respectively. For the remainder of the article, we refer to these stretch rates as frequency values (1Hz and 5Hz) to relate the ramping speed to a stretch-rate corresponding to the heart rate in sub- and physiological conditions. Between each test, a recovery time of ten times that of the previous testing period was included to ensure full recovery of the tissue from the previous test [25]. Biaxial stretch forces were obtained by 5-lb load cells (Honeywell) at a sampling frequency of 200 Hz. Because only stress-time curves were used to analyze the viscoelastic behavior of the tissue, we did not obtain the local strain of the tissue in our experimental procedures. After the intact tissue was tested at the baseline condition (base), the RV was exposed to 0.3mM colchicine [17] (COL) for 30 minutes to de-polymerize the MT, and the same mechanical testing was performed. The effect of COL is transient [26] and we therefore were not able to perform immunofluorescence imaging to determine the

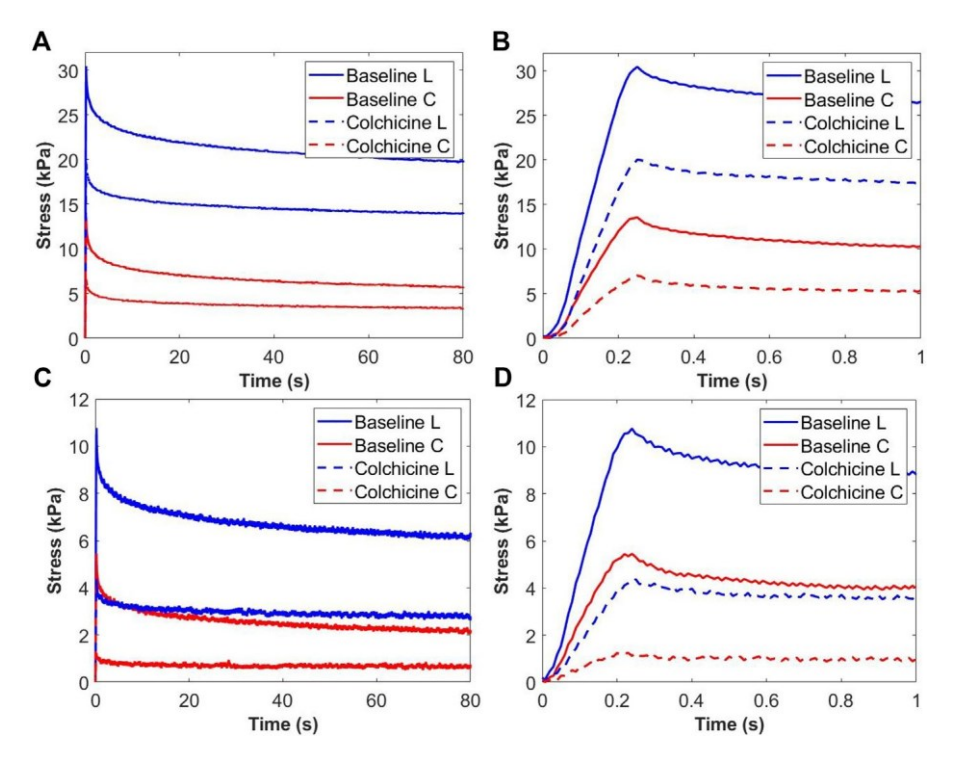


Fig. 1. Representative stress relaxation curves at baseline and after colchicine treatment in the longitudinal (L) and circumferential (C) directions at 15% strain (A&B) and 6% strain (C&D). The total response curve is given in panels A&C, and the ramping region is shown in panels B&D.

degree of MT de-polymerization. Representative stress-time curves before and after colchicine treatment in both groups are shown in Figure 1, and the peak stress values for each group are presented in Supplemental Table S1. Finally, because the colchicine's effect is transient, the baseline stress-strain curves were measured at the end of the experiment and compared to those obtained in the beginning of the experiment. We did not observe any plastic damage to the tissue samples.

2.3. Data analysis

After data collection, the 2^{nd} Piola-Kirchhoff (PK) (**S**) stresses and Green strain (**E**) were derived as described previously [7,27]:

$$\mathbf{S} = (\mathbf{F}/A_0)\boldsymbol{\lambda} \tag{1}$$

$$\boldsymbol{E} = \frac{1}{2} \boldsymbol{\lambda}^2 - 1^{)}, \tag{2}$$

where F is the measured force, A_{θ} is the initial cross-sectional area, and λ is the stretch.

Next, we quantified RVFW elasticity and viscosity from the stress relaxation curve (Fig. 2) using stored energy (W_S) and dissipated energy (W_d), respectively [21,28]. At a given input strain (\mathcal{E}_{input}) level, W_S was derived as a function of time (t) using the total area (A_S) under the curve from the peak stress to the fully relaxed stress at time t (Eq. 1). W_d was derived using the area (A_d) between the raw stress-relaxation curve and the purely elastic material response curve from the peak stress (S_p) to the relaxed stress at time t (Eq. 2) [28]. We then calculated the ratio of viscosity to elasticity (V/E) as the ratio of dissipated to stored energy (W_d/W_S) to measure the relative contribution of viscosity. For convenience, only the results at 100s after peak stress (equilibrium state) are presented in our Results.

$$W_{S}(t) = \int_{t_{p}}^{t} S(t) \, \mathcal{E}_{input} dt = \, \mathcal{E}_{input} \int_{t_{p}}^{t} S(t) \, dt = \, \mathcal{E}_{input} \times A_{S}$$
 (3)

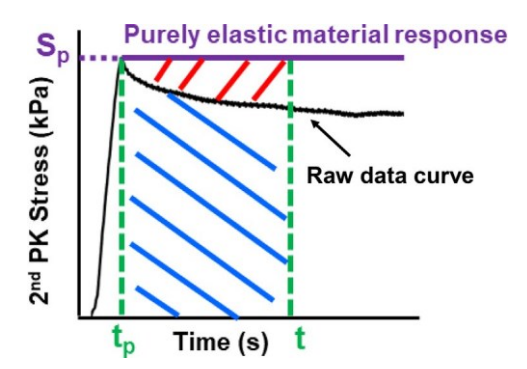


Fig. 2. The stored energy (W_S) and dissipated energy (W_d) are derived from the blue (A_S) and red (A_d) shaded area, respectively. These integrated areas (A_S) and A_d are calculated between the time (t_p) of peak stress (S_p) and any time point (t) during relaxation.

$$W_d(t) = \int_{t_p}^t S_p \varepsilon_{input} dt - \int_{t_p}^t S(t) \varepsilon_{input} dt$$

$$= \varepsilon_{input} \int_{t_p}^t S_p dt - \int_{t_p}^t S(t) dt = \varepsilon_{input} \times A_d$$
(4)

Relaxation modulus and normalized stress were also derived as described previously [7,21], and they are presented in **Supplemental Tables S2 and S3**.

24. Constitutive model of tissue viscoelasticity: Quasilinear viscoelastic fitting

To further characterize the viscoelastic behavior, an established QLV model was used to fit the experimental data as previously de-

scribed [6,28]. Assuming incompressibility and negligible shear deformation, the QLV construction for the 2^{nd} PK stress tensor (S) can be presented as [29]:

$$\mathbf{S}(\mathbf{E},t) = \mathbf{S}_0 + \int_0^t \mathbf{G}(t-\tau) \frac{\partial \mathbf{S}^e}{\partial \mathbf{E}} : \frac{\partial \mathbf{E}(\tau)}{\partial \tau} d\tau$$
 (5)

where **E** is the Green strain tensor, t is time, S_0 is the initial stress pretension obtained from the force in the zero-stress configuration, which was set to zero [29–31], G(t) is the reduced relaxation function, S^e is the instantaneous elastic stress, and τ is a time variable of integration. The Green strain tensor (**E**) was prescribed by the global position of the actuators, with linear increments during the ramp period and held fixed during the relaxation period. Only normal (longitudinal and circumferential) strains were applied, and shear strains were negligible at the boundaries at all times. The anisotropic Ogden strain energy density function (ψ) was used to derive the instantaneous elastic stress S^e [31,27]:

$$\psi = \frac{2\mu}{\alpha^2} \lambda_1^{\alpha} + \lambda_2^{\alpha} + \lambda_3^{\alpha} - 3 + \frac{2k\mu}{\alpha^2} I_4^{\frac{\alpha}{2}} + I_4^{-\frac{\alpha}{4}} - 3$$
 (6)

using

$$\mathbf{S}^{\mathbf{e}} = 2\frac{d\psi}{dC} - p\mathbf{C}^{-1} \tag{7}$$

where the parameters α , μ and k represent the nonlinearity, infinitesimal shear modulus and anisotropy of the tissue, respectively. The principal stretch λ_i are the diagonal elements of the deformation gradient tensor when no shearing is present. C is the right Cauchy-Green deformation tensor, and C=2E+I. With the L and C directions aligned to the λ_L and λ_C , respectively, the anisotropic invariant I_4 was equal to:

$$I_4 = \mathbf{a}_0 \cdot \mathbf{C} \mathbf{a}_0 = \lambda^2 \cos O^2 + \lambda^2 \sin O^2$$
 (8)

where \mathbf{a}_0 is a vector describing the fiber orientation defined by the angle Θ , and $\Theta = 0$ represents the fiber aligned along the longitudinal (outflow tract) direction.

In this study, the reduced relaxation function G(t) in each direction was defined by the Prony series as:

$$G(t) = G_{\infty} + \sum_{n=1}^{\infty} G_n e^{-t/\tau_n}$$
(9)

such that:

$$G_1 + G_2 + G_3 + G_{\infty} = 1 \tag{10}$$

where G_{∞} is the long-term relaxation coefficient, which quantifies the proportion of instantaneous elastic stress S^e remaining in the RVFW over a long (infinite) period. G_n are relaxation coefficients corresponding to the following time constants in the relaxation: $\tau_1 = 0.3$ s, $\tau_2 = 3$ s, and $\tau_3 = 30$ s. These time constants were selected because they have been shown to successfully fit ovine RVFW viscoelastic behavior. Each G_n represents the relaxation strength at the corresponding time constant. Representative fitting results are presented in **Supplemental Figures S2 and S3**, and the root mean-squared error values are provided in **Supplemental Table S4**.

2.5. Statistical analysis

The normal distribution of the data was confirmed by Shapiro-Wilk test. Unpaired and paired student t-tests were used to compare disease effect, stretch rates, strain level, directions, and before

and after MT de-polymerization. All data are presented as mean \pm SEM. P<0.05 was considered statistically significant.

3. Results

3.1. Pulmonary hypertension increases RVFW viscosity and elasticity at sub- and physiological stretch rates as well as early and late diastolic strains

We firstly examined the change in wall thickness between healthy and diseased RVs and observed significant wall thickening in the PH tissues, with a thickness of 1.0mm \pm 0.05 mm in the healthy tissues, and 1.4mm \pm 0.1 mm in the diseased tissues, indicating marked hypertrophy of the myocardium consistent with our previous report [21]. Next, we investigated the effect of pulmonary hypertension on RVFW viscoelasticity at the early and end diastolic strain level, and at the sub- and physiological stretch rates. At the early diastolic strain level (6%) and sub-physiological stretch rate (1Hz), RVFW elasticity (W_S) and viscosity (W_d) were elevated during PH progression (Fig. 3A&C). The degree of increase in W_d was greater than W_S in the circumferential direction, which resulted in an elevated V/E ratio in this direction with PH (Fig. 3C). At the early diastolic strain (6%) and physiological stretch rate (5Hz), we observed strengthened RVFW elasticity (Ws) and viscosity (W_d) in both directions with the development of PH, and the increases (in percentage) were larger in the circumferential than longitudinal direction (Fig. 3D&E). A decrease of the V/E ratio with PH progression was observed, but the change reached significance in the longitudinal direction only (Fig. 3F). Next, we examined RVFW viscoelasticity at late diastolic strain (15%) and physiological stretch rate (5Hz). Similarly, as found in the low strain tests, tissue elasticity and viscosity were enhanced with PH progression, and the increases (in percentage) were stronger in the circumferential than longitudinal direction (Fig. 3G&H). However, the V/E ratio was not significantly changed by PH progression in either direction (Fig. 3I). Finally, all W_S and W_d obtained from these testing conditions showed significant anisotropy in healthy and failing RVs.

3.2. Diseased RV and healthy RV exhibit different stretch-rate dependent elasticity and viscosity

Next, we investigated the effect of stretch rate on the healthy and diseased RV elasticity (W_S) and viscosity (W_d). Increasing from a sub-physiological to a physiological stretch-rate did not influence healthy RV elasticity in either direction, but it significantly increased diseased RV elasticity in both directions (Fig. 4A&B). In contrast, when examining the stretch-rate's effect on tissue viscosity, we found that the viscosity of healthy and diseased RVs was increased significantly in both directions (Fig. 4C&D). The percentage of increase in W_d was more pronounced in the healthy RV (L=35%, C=42%) than diseased RV (L=11%, C=18%). Our results showed that the stretch-rate had a greater effect on the viscosity of healthy RVs and the elasticity of the diseased RVs.

33. Diseased RV and healthy RV exhibit similar strain dependent elasticity and viscosity

Additionally, we analyzed RVFW viscoelasticity at a physiological stretch rate and at early and end diastolic strain levels. As expected, we observed increased viscosity and elasticity of the RVFW from the early to the end diastolic strain levels (Fig. 5), indicating the strain stiffening and strain "thickening" effects of the tissue. This behavior was observed in both the healthy and the diseased

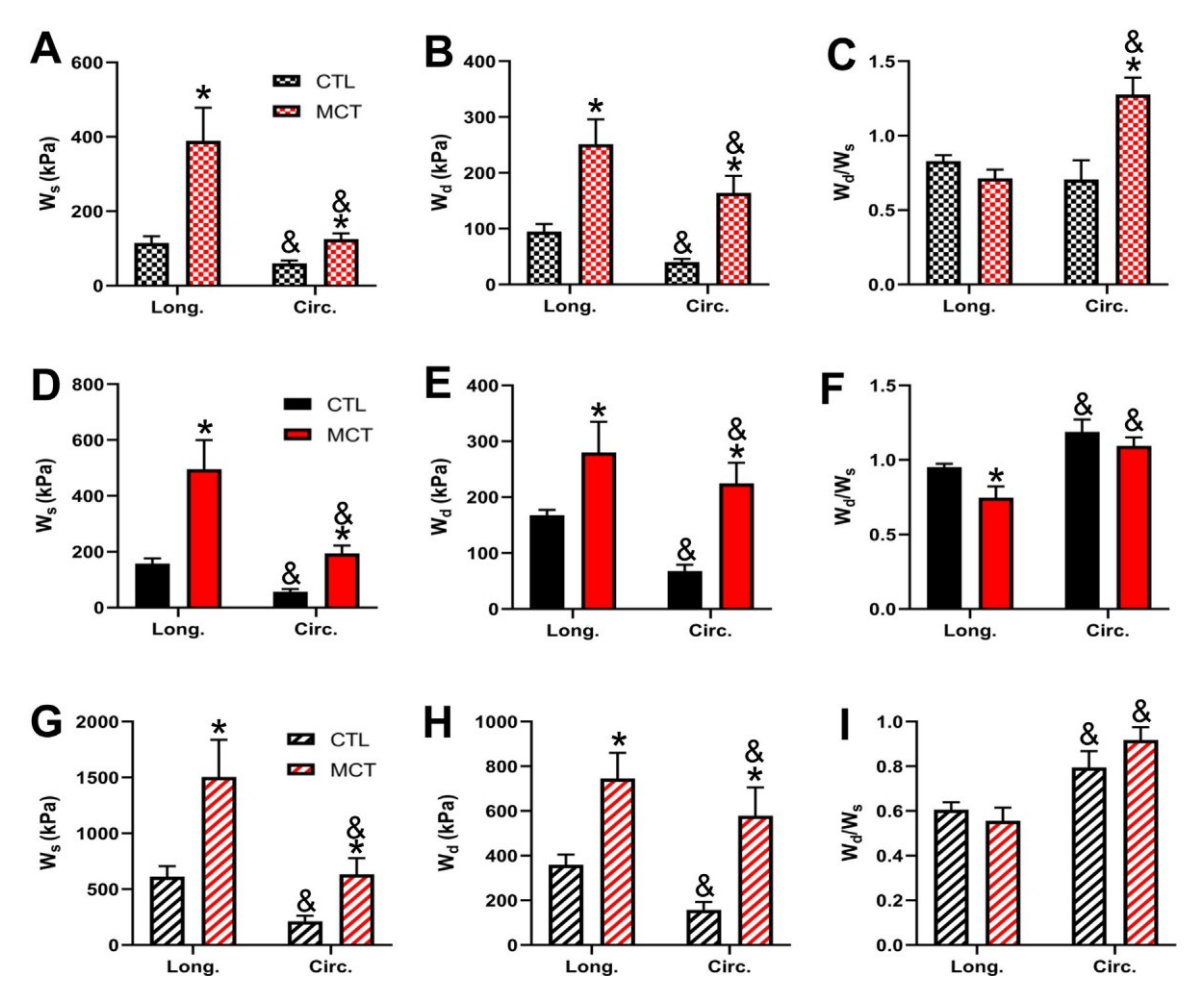


Fig. 3. The elasticity (W_S) (A, D, G), viscosity (W_d) (B, E, H), and the V/E ratio (C, F, I) of the healthy and diseased RVFW that are obtained at sub-physiological stretch rate and early diastole strain level (A-C), physiological stretch rate and early diastolic strain level (D-F), and physiological stretch rate and end diastolic strain level (G-I). *p<0.05 compared to CTL in same direction; & p<0.05 compared to L direction in same group.

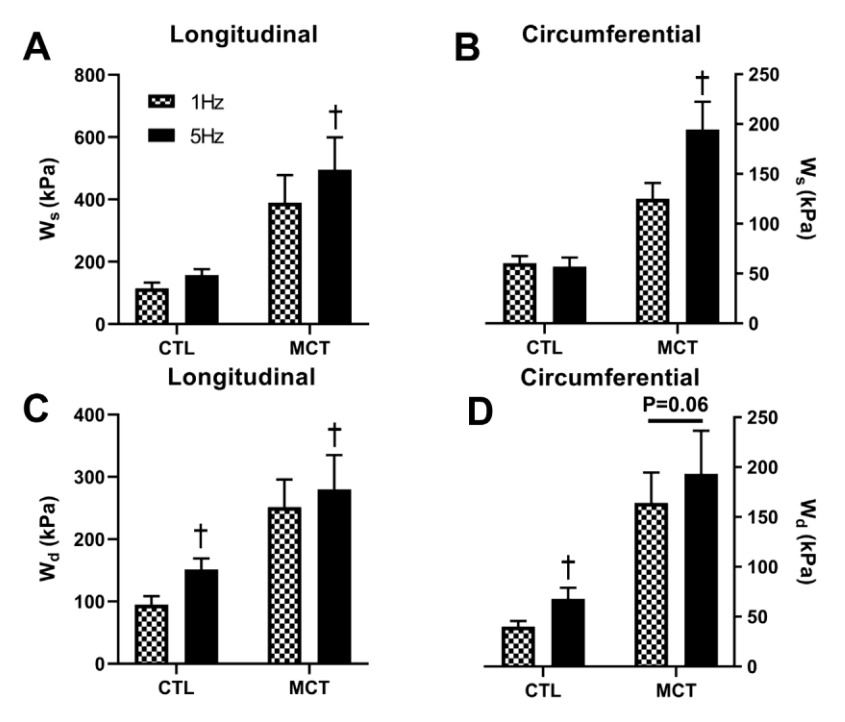


Fig. 4. The elasticity (W_S) (A&B) and viscosity (W_d) (C&D) of healthy and diseased RVFW in the longitudinal (left column) and circumferential (right column) directions at the sub-physiological (1Hz) and physiological (5Hz) stretch rates. † p<0.05 compared to the sub-physiological stretch rate.

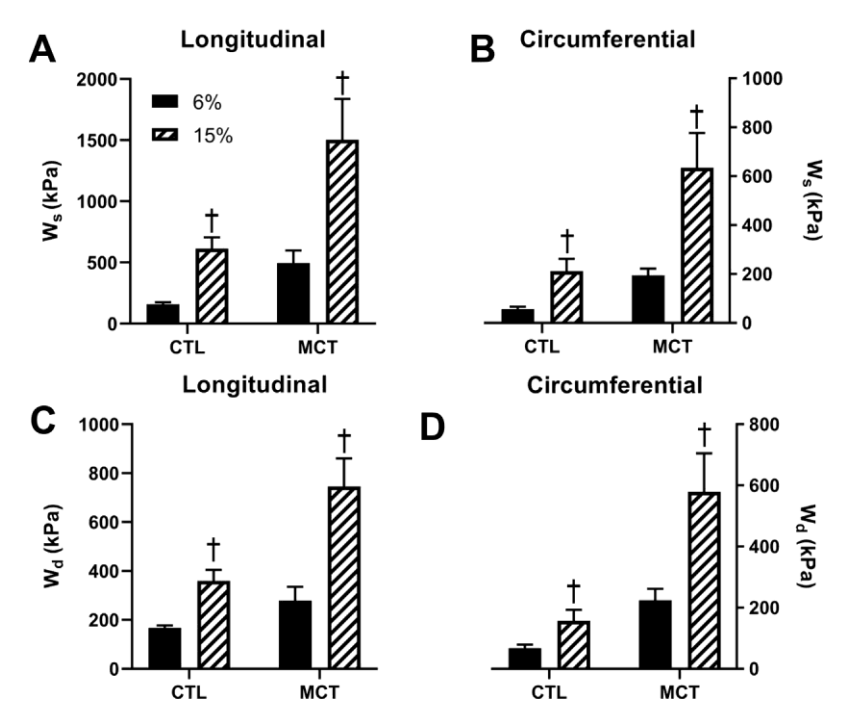


Fig. 5. The elasticity (W_S) (A&B) and viscosity (W_d) (C&D) of healthy and diseased RVFW in the longitudinal (left column) and circumferential (right column) directions at the early diastolic (6%) and end diastolic (15%) strain levels. † p<0.05 compared to the early diastolic strain level.

RVFW, suggesting that the impact of strain level on myocardial mechanics is independent of health states.

3.4. Removal of MT similarly weakens viscoelasticity of diseased RV and healthy RV at early diastolic strain

After examining how PH impacts on RVFW viscoelasticity, we investigated the contribution of the MT network to healthy and diseased RVs firstly at the early diastolic strain level. Because the mechanical behavior at physiological stretch rate is more relevant to organ performance, we only present the data obtained from this condition from now on. First, in both directions, the elasticity (W_S) and viscosity (W_d) were significantly reduced in both groups after MT removal Fig. 6A&B, D&E), except for a moderate trend of reduction of elasticity in the diseased RVFW in the longitudinal direction (p=0.1). However, the degrees of reduction were direction dependent. In the healthy RV, the degree of change in elasticity was stronger in the longitudinal than circumferential direction, whereas the degree of change in viscosity was equivalent between directions (Table 1). Alternatively, in the diseased RV, elasticity was reduced more greatly in the circumferential than the longitudinal direction. This behavior was also present in viscosity (Table 1). Moreover, the V/E ratio was reduced significantly in both directions and for both groups (Fig. 6C, F). This result is due to the greater reduction of viscosity than elasticity, indicating a stronger role of the MT network in tissue viscosity (Fig. 6C).

Table 1 Degree of reduction in healthy and diseased RV elasticity (W $_{\rm g}$) and viscosity (W $_{\rm d}$) after the disruption of the MT network via colchicine at 6 % strain. Reductions were derived from group average values. Long.: longitudinal; Circ.: Circumferential.

Parameter	Healthy RV		Diseased RV	
	Long.	Circ.	Long.	Circ.
Stored energy (Ws)	34%	18%	33%	41%
Dissipated energy (W _d)	48%	43%	30%	60%

3.5. Removal of MT differently weakens viscoelasticity of diseased RV and healthy RV at end diastolic strain

It is found that the elastic behavior of myocardium is dominant by myofibers at small strains and by collagen fibers at large strains [3]. But whether and how much the MT network contributes to the tissue-level viscoelasticity at larger strains is unclear. To answer this question, we investigated the effects of MT removal on RV viscoelasticity at the end diastolic strain level. In contrast to the results at early diastolic strain, we observed a differential role of the MT network in the healthy and diseased RVs. First, in the longitudinal direction, both elasticity and viscosity were weakened after MT removal in the healthy RVs, but this change was not observed in the diseased RVs (Fig. 7A&B). Moreover, there was an absent effect on the V/E ratio for both groups (Fig. 7C). In the circumferential direction, the effects of MT removal on elasticity and viscosity were similar between healthy and diseased RVs - no change on elasticity but a decrease of viscosity were noted (Fig. 7D&E). Unlike at early diastole, the degrees of reduction in elasticity and viscosity were not direction dependent anymore. We observed similar percent reductions in tissue elasticity and viscosity in both directions for both groups (Table 2), except that in the pressureoverloaded RV, we observed a much larger decrease (~2-fold) in circumferential viscosity compared to that in the longitudinal direction (Table 2). Additionally, the MT removal led to a reduction in the V/E ratio in the diseased RVs only (Fig. 7F). These results suggest distinct contributions of MT network to the viscoelasticity of normotensive and hypertensive RVs after collagen recruitment.

Table 2 Degree of reduction in healthy and diseased RV elasticity (W 3) and viscosity (W 3) after the disruption of the MT network via colchicine at 15% strain. Reductions were derived from group average values. Long.: longitudinal; Circ.: Circumferential.

Parameter	Healthy RV		Diseased RV	
	Long.	Circ.	Long.	Circ.
Stored energy (Ws)	15%	14%	16%	17%
Dissipated energy (W _d)	20%	18%	15%	30%

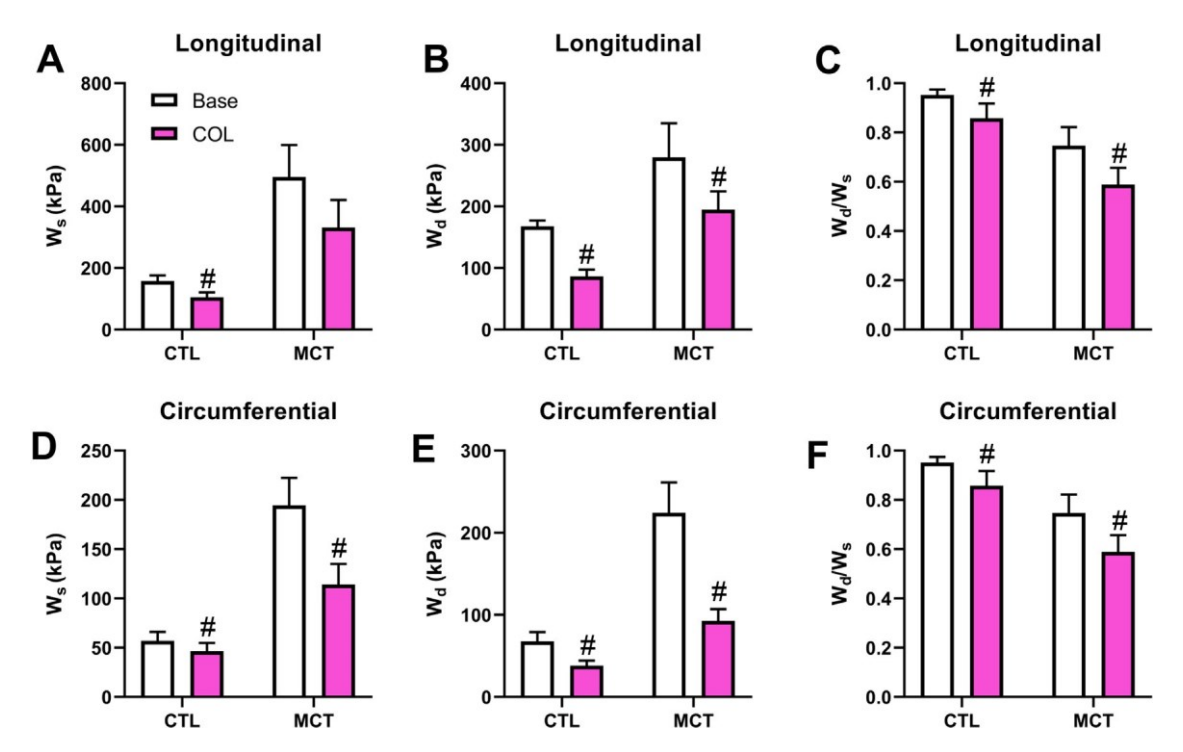


Fig. 6. The elasticity (A&D), viscosity (B&E), and the V/E ratio (C&F) of healthy and diseased RVFW after the removal of the MT network (COL) under 6% strain and ramp speed corresponding to 5Hz. #p<0.05 compared to baseline in same direction and group.

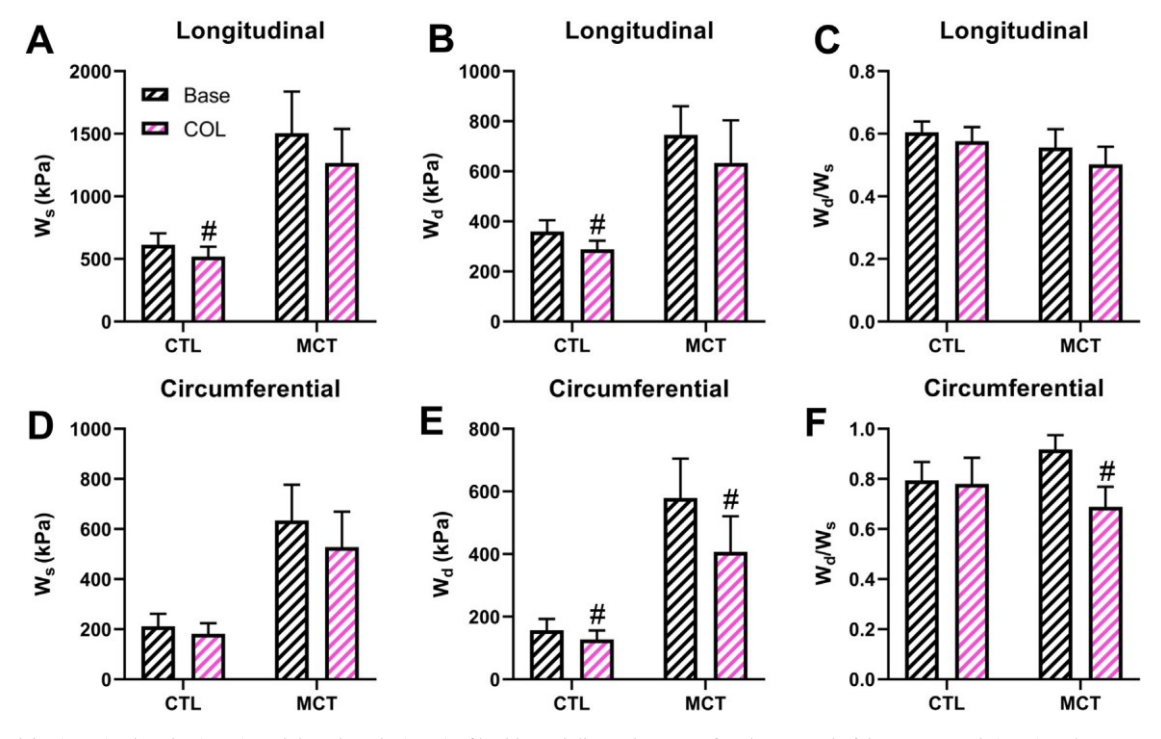


Fig. 7. The elasticity (A&D), viscosity (B&E), and the V/E ratio (C&F) of healthy and diseased RVFW after the removal of the MT network (COL) under 15% strain and ramp speed corresponding to 5Hz. #p<0.05 compared to baseline in same direction and group.

3.6. QLV modeling reveals removal of MT network decreases RV relaxation strength (viscosity) at late time points of relaxation in healthy and diseased RVFW

Lastly, we applied a QLV model to characterize the role of MT in the relaxation behavior of the RVFW with disease progression and removal of MT. First, at the early diastolic strain level, tissue relaxation strength at a later time point (G_3) was reduced after

the removal of the MT network in both directions and for both groups (Fig. 8A&B). Similar effects were observed at the end diastolic strain level (Fig. 8C&D). These data suggest that the G_3 coefficient is affected by the MT network, regardless of the strain levels or disease state. Moreover, we found that G_2 was reduced in the diseased RVs as well, and the reduction was in the longitudinal direction at early diastolic strain (Fig. 8A) and in the circumferential direction in the end diastolic strain (Fig. 8D).

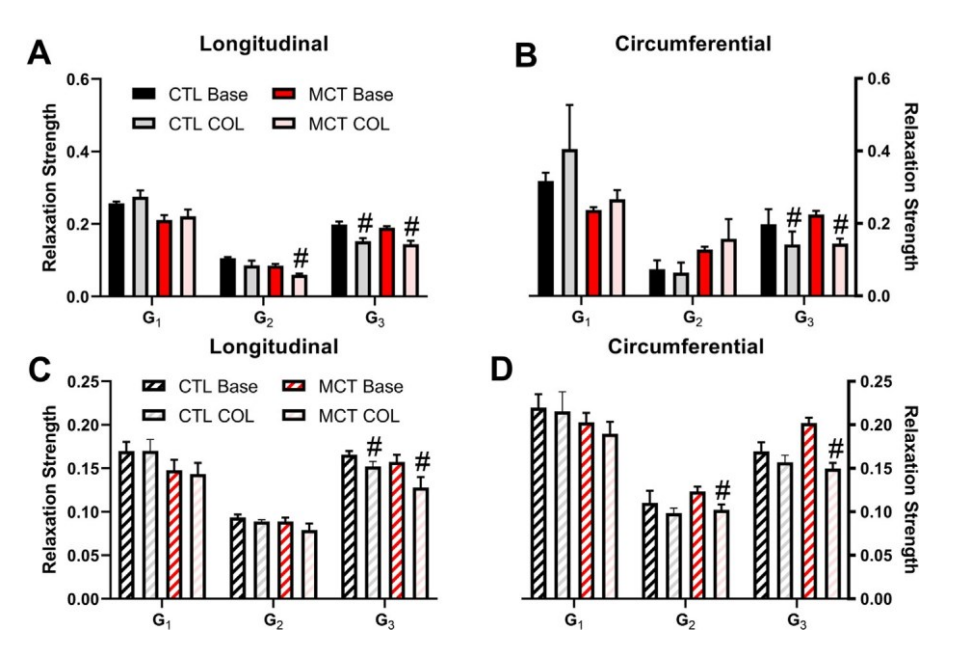


Fig. 8. The relaxation strength (G_n) of healthy and diseased RVFW before and after the removal of the MT network at early (A&B) and end (C&D) diastolic strain levels. #p<0.05 compared to baseline in same group and direction.

The QLV modeling also revealed elevated shear modulus with disease progression at both strain levels (Supplemental Figures S4A & S5A). Additionally, shear modulus was reduced in the diseased RV (at 6% strain) and the healthy RV (at 15% strain) after removal of the MT network (Supplemental Figures S4A & S5A). Tissue nonlinearity was increased in healthy RVs after MT removal (Supplemental Figure S4B). We did not observe marked changes in other fitting parameters, indicating limited effect of disease progression or the MT network on nonlinearity and anisotropy.

4. Discussion

To our knowledge, this is the first tissue-level examination of the role of the MT network in the anisotropic viscoelasticity of the failing RV. We originally observed 1) PH progression elevated RVFW elasticity and viscosity, and the increase was stronger in the circumferential than longitudinal directions; 2) the stretch rate, not strain level, differently affected the elasticity and viscosity of the healthy and diseased RVs; 3) at the early diastolic strain level, the removal of MT network reduced tissue elasticity, viscosity, and the ratio of viscosity to elasticity in both directions and for both healthy and diseased RVs; 4) at the end diastolic strain level, the removal of MT network reduced viscosity and elasticity in healthy RVs, but it only reduced the circumferential viscosity and the ratio of viscosity to elasticity in diseased RVs. The new findings of the role of the MT network in the failing RV tissue mechanics strengthen our knowledge of RV viscoelastic behavior and deepen the understanding of microstructural determinants of RV failure.

4.1. PH altered RVFW anisotropic elasticity and viscosity

The hemodynamic measurements reported in our previous study clearly demonstrate an establishment of RV failure with PH progression in these rats [21]. From our baseline mechanical data, the development of PH significantly enhanced RVFW elasticity and viscosity (Fig. 3), and this effect was present at the sub- and physiological stretch rate and at both the early and end diastolic strain levels. Similar findings of enhanced viscoelasticity with disease progression have been reported previously at the tissue and cellular level [13,14,17,21,32,33].

Moreover, in the present study, we have new findings in the tissue anisotropy and stretch-rate/strain dependent changes. The RVFW displayed strong anisotropic behavior in the healthy and diseased states, with larger elasticity and viscosity in the longitudinal direction (Fig. 3). Similar trends have been reported in our previous study [21]. During PH progression, the myo- and collagen fibers realign into a preferred direction toward the longitudinal (outflow tract) direction [3-5]. Thus, this may be the underlying cause of the stronger elasticity and viscosity in the longitudinal direction. Furthermore, the effect of disease progression on the V/E ratio was direction and stretch rate dependent. At the sub-physiological stretch rate, the V/E ratio was strengthened by PH in the circumferential direction (Fig. 3C), which is a result of a weaker increase in elasticity than viscosity. Alternatively, the V/E ratio at the physiological stretch rate was weakened in the longitudinal direction (Fig. 3F) as a result of greater increase in elasticity than viscosity. We do not know exactly the mechanism causing the stretch-rate dependent changes in V/E ratio, but this is consistent with our findings of different effects of stretch-rate on healthy and diseased RV viscoelasticity (Fig. 3), as discussed below. The results suggest that it is imperative to obtain myocardium tissue viscoelasticity under physiologically relevant conditions.

42. Altered stretch-rate dependent changes in RVFW elasticity and viscosity with PH progression

Biological tissues are viscoelastic, and this behavior can be either strain or strain-rate dependent [34]. Caporizzo et al. found at the cellular level that isolated healthy cardiomyocytes exhibit enhanced elastic modulus and stronger hysteresis behavior under a diastolic (10% over 5s) compared to a sub-physiological stretch speed (10% over 200ms) [17]. While stretch-rate dependence has been reported in the healthy myocardium, [8,9,32], the observations are not consistent. Sommer et al. studied the mechanical behavior of human LV and RV and found that the viscosity (hysteresis loop area) is greater at the dynamic (30mm/min) stretch rate compared to the quasi-static (3mm/min) stretch rate [9]. However, the elastic modulus (slope of the loop), was unchanged between stretch rates. Our results here showed similar behavior in the healthy RVFW, with no change in elasticity (Ws) (Fig. 4A&B)

but an increased viscosity (W_d) (Fig. 4C&D) with increasing stretch rate. However, there is a different story in the diseased RVFW, with both elasticity and viscosity increasing from the sub- to physiological stretch rates (Fig. 4). Our group has previously shown stronger stretch-rate dependent behavior in the diseased RV compared to the healthy RV [21]. Relaxation modulus, a metric of overall viscoelasticity, monotonically decreased with increasing frequency and this trend was stronger in the PH group. However, these measurements were taken at the beginning of relaxation (0.01s after peak stress), whereas our results here were obtained at the end of relaxation (100s after peak stress). Moreover, in the diseased RVs, there is an accumulation of collagen, and the enhanced contribution of collagen may be responsible for the stretch-rate dependent elasticity seen in the diseased RVs. Further investigation is needed to de-couple the roles of cellular and extracellular components in tissue mechanics.

43. Effects of MT network on RVFW elasticity and viscosity with disease progression at early diastolic strain

At the early diastolic strain level, we observed reduced elasticity and viscosity after MT removal in both directions and for both groups. This indicates that the MT network is an important component conferring the viscoelastic behavior of the tissue. Besides, we observed other interesting findings when comparing the reductions between directions and between groups. Firstly, we noted that in the healthy RVs, the reduction of viscosity was equivalent between directions (~43%), while the decrease in elasticity was stronger in the longitudinal direction (~34%) compared to the circumferential direction (~18%) (Fig. 6A-C). This suggests that the contribution of MT is isotropic for tissue viscosity but anisotropic for tissue elasticity. However, in the diseased RVs, the drops in viscosity (59%) and elasticity (24%) were both greater in the circumferential than longitudinal (30% and 5% for viscosity and elasticity, respectively) direction (Fig. 6D-F). Thus, the contribution of MT is anisotropic for both mechanical properties, and this indicates an altered MT microstructure or organization in the diseased RV, as reported by Prins et al [20]. In healthy cardiomyocytes, the MT network forms an orthogonal grid, where the cytoskeletons are predominantly aligned along the axis of the cell with interspersed transverse structures that run perpendicular to the cell axis [35]. With PH progression, though, the cardiomyocytes have a preferred alignment along the outflow tract (longitudinal) direction [3-5], and the MT network density is increased and less organized [20]. The disorganization of the MT network may lead to a failure of the cytoskeletons to keep aligned with the axis of the cell as in healthy state, and the transverse MT component becomes more prominent in the diseased RVs. Therefore, the greater reduction of viscosity and elasticity occurred in the circumferential direction after the MT depolymerization in these tissues. It should be acknowledged, too, that the alignment behavior of titin - a large sarcomeric protein - is altered with disease progression [5,36] and may be adversely affected by the breakdown of the MT network. We cannot rule out this secondary effect of MT removal, which awaits further investigations. Overall, despite the same trend (reduction) found in healthy and diseased RVs after MT depolymerization, the accumulation and altered microstructure of MT network have resulted in distinct impacts on RVFW mechanics with disease progression.

4.4. Effects of MT network on RVFW elasticity and viscosity with disease progression at end diastolic strain

We have shown that the removal of the MT network significantly reduced healthy and diseased RVFW elasticity and viscosity at the early diastolic strain level (Fig. 6), which is consistent with the results of isolated cardiomyocytes [15,17,33]. However,

when examining the effects of MT network at the end diastolic strain level, the healthy and diseased RVFW exhibited different responses: the removal of MT network reduced viscosity and elasticity in healthy RVs, but it only reduced the circumferential viscosity and the ratio of viscosity to elasticity in diseased RVs. (Fig. 7).

When the mechanical characterization is mainly performed for cardiomyocytes (at cell or fiber levels), the behavior is mainly attributed to the cellular components such as MT or titin. However, when the mechanical characterization is performed at the tissue level, the deformation will incorporate other non-cellular components (especially at large strains) and the overall behavior is a combined contribution of all tissue components. It must be considered, at the higher strain level, that collagen is recruited and having a greater contribution to myocardial mechanics than myofibers [3,37]. Therefore, we investigated the effects of MT at both 6% and 15% strains in this study to reveal the contribution of MT at myofiber-dominant and non-dominant regions. Not surprisingly, we observed different effects of MT network at early (6%) and end (15%) diastolic strain levels. As we found and discussed above for the results at early diastolic strain, in the healthy RV, the axial MT may contribute more to the elasticity and viscosity than the transverse MT, resulting in a stronger role of the MT in the longitudinal direction. A similar effect of MT remains evident in the healthy RV even after collagen recruitment (Fig. 7). But the effects of MT on diseased RVs at the large strain were different than those at small strain. The viscoelasticity in the longitudinal direction was totally unchanged in these RVs, indicating a non-significant role of MT after collagen accumulation (due to PH) and recruitment (due to large strain). There were still some effects of MT in the circumferential viscosity and the V/E ratio (Fig. 7E&F), though. We speculate that this may be related to the increased transverse MT component (as discussed above) in the diseased RVs as well as the intrinsically larger viscosity in MT network than collagen fibers. Nevertheless, the results suggest that the contribution of MT to tissue viscosity is significant, even after the collagen recruitment. As prior cell studies have shown an increased contractile function of cardiomyocytes with reduced cell viscoelasticity [13], the role of tissue viscosity should not be ignored in ventricular performance and new therapies may consider targeting MT polymerization in RV failure patients [35].

45. QLV modeling shows the role of MT in RV relaxation strength in disease progression is strain-dependent

In addition to our findings from the experimental data, the computational work provides further insights into the role of the MT network in the relaxation behavior of the RVFW. As established in our prior work [6], we used three terms of relaxation coefficients (G_n) to capture the relaxation strength of the RV. We observed that the removal of MT network significantly reduces RV relaxation strength (viscosity) at the late time point (G₃) in both healthy and diseased RVs and at both strain levels (Fig. 8). These results not only demonstrate a strong contribution of the MT to the RV tissue viscosity in both directions, but also delineate the specific time scale of its contribution. Unfortunately, although the Fung's QLV theory has been applied to various biological and nonbiological materials, to our knowledge, how the G_n is correlated to specific component (e.g., MT, collagen) or microstructure (e.g., size of fiber, bonds) of a material remain largely unknown. Nordsletten et al. has proposed that the hierarchical structure of the extracellular matrix (mainly collagen) is responsible for the molecular mechanism of relaxation at different time scales- from fibrils, to fibers, to bundles to sheets - in human myocardium [38]. Our results suggest that MT is responsible for the G₃ in both healthy and diseased RVs. We did observe some changes in G2 in the diseased RV as well. For instance, the longitudinal G₂ at small strain and the

circumferential G_2 at large strain were reduced after MT removal. We do not exactly know the reason for these changes, and future study may investigate the microstructure and proliferation of MT under pressure overload to reveal the molecular mechanism.

5. Limitations

We did not perform immunofluorescence imaging to assess the degree of microtubule disruption after colchicine treatment. This is because the drug effect is reversible, and we need to obtain the baseline data at the end of experiment to ensure no damage to the tissue during the mechanical test. However, we performed a dose response study to determine the dose used in this work, which resulted in a marked drop in peak stress (Fig. 1). Our results are also consistent with the response observed at the cell level [13,17,19]. Additionally, calipers were used for thickness measurement, and it is possible that tissue was squeezed during the procedure, which may affect the accuracy of the measurement. While other more accurate methods are available, this procedure is quick and allows us to obtain the tissue viscoelastic behavior in a fresh state. Finally, in the data analysis, we did not use the local strain, but rather the input (global) strain. Previous studies have shown that the use of local strain/deformation provided improved fitting capabilities of the model than the use of global strain/deformation [30,39]. We did not acquire image data during the stress-relaxation testing and, therefore, we were unable to obtain the local strain/deformation. Nevertheless, the QLV model still offered strong fitting capabilities at both the 6% and 15% strain levels.

6. Conclusions

This is the first study to investigate the role of the microtubules in the passive viscoelasticity of the RVFW in pulmonary hypertension progression. We found that PH increased RV elasticity and viscosity, and the increase was stronger in the circumferential than longitudinal directions. The stretch rate, not strain level, differently affected the elasticity and viscosity of the healthy and diseased RVs. The removal of the MT network weakened healthy and diseased RV viscoelasticity at the early diastolic strain level, but it only reduced the circumferential viscosity and the ratio of viscosity to elasticity in diseased RVs. These results suggest that the impact of MT on tissue viscoelasticity is different at small and large deformations, which contributes to the nonlinear behavior of the tissue. This is the first study to demonstrate the effect of MT accumulation on tissue mechanics of hypertrophied RVFW. Future work can investigate the functional decline of the organ due to viscoelastic changes and inspire therapies targeting microtubules in RV failure patients.

Declaration of competing interest

The authors declare that they have no known competing financial interests or personal relationships that could have appeared to influence the work reported in this paper.

Funding

This work is supported by the National Science Foundation (NSF) grant 2244994.

Author contributions

KL and ZW designed and managed the study; KL performed the experiments, acquired and analyzed the data, and constructed the draft of the manuscript; JP assisted with the disease model and animal care. WL, AJC, JP, and ZW assisted with the interpretation

of the data and revised the manuscript; all authors have reviewed and approved this work.

Data availability

All raw and analyzed data are available upon request. Please email Kristen LeBar (Kristen.lebar@colostate.edu) for access.

Supplementary materials

Supplementary material associated with this article can be found, in the online version, at doi:10.1016/j.actbio.2024.01.023.

References

- S.S. Virani, Connie.W. Tsao, Heart disease and stroke statistics-2020 update: a report from the american heart association, Circulation 141 (9) (2020).
- [2] W. Liu, et al., Correlations between the right ventricular passive elasticity and organ function in adult ovine, J. Integr. Cardiol. 6 (2020) 1–6, doi:10.15761/JIC. 1000294.
- [3] S. Jang, et al., Biomechanical and hemodynamic measures of right ventricular diastolic function: translating tissue biomechanics to clinical relevance, J. Am. Heart. Assoc. 6 (9) (2017), doi:10.1161/JAHA.117.006084.
- [4] W. Liu, Z. Wang, Current understanding of the biomechanics of ventricular tissues in heart failure, Bioengineering 2020 7 (1) (2019) 2 Vol. 7, Page 2, doi:10.3390/BIOENGINEERING7010002.
- [5] M.R. Hill, M.A. Simon, D. Valdez-Jasso, W. Zhang, H.C. Champion, M.S. Sacks, Structural and mechanical adaptations of right ventricle free wall myocardium to pressure overload, Ann. Biomed. Eng. 42 (12) (2014) 2451–2465, doi:10. 1007/s10439-014-1096-3.
- [6] W. Liu, et al., Strain-dependent stress relaxation behavior of healthy right ventricular free wall, Acta Biomater. 152 (2022) 290–299, doi:10.1016/J.ACTBIO. 2022.08.043
- [7] L. W, N.-T. M, A. M, L. KM, P. CM, W. Z, Different passive viscoelastic properties between the left and right ventricles in healthy adult ovine, J. Biomech. Eng. 143 (12) (2021), doi:10.1115/1.4052004.
- [8] F. Ahmad, et al., Biomechanical properties and microstructure of neonatal porcine ventricles, J. Mech. Behav. Biomed. Mater. 88 (2018) 18–28.
- [9] S. G, et al., Biomechanical properties and microstructure of human ventricular myocardium, Acta Biomater. 24 (2015) 172–192, doi:10.1016/J.ACTBIO.2015.06.
- [10] L.L. Demer, F.C. Yin, Passive biaxial mechanical properties of isolated canine myocardium, J. Physiol. (1983).
- [11] M.A. Caporizzo, B.L. Prosser, The microtubule cytoskeleton in cardiac mechanics and heart failure, Nat. Rev. Cardiol. 19 (6) (2022) 364–378, doi:10.1038/S41569-022-00692-Y.
- [12] M.A. Caporizzo, B.L. Prosser, Need for speed: the importance of physiological strain rates in determining myocardial stiffness, Front. Physiol. 12 (2021), doi:10.3389/FPHYS.2021.696694.
- [13] M.A. Caporizzo, C.Y. Chen, A.K. Salomon, K.B. Margulies, B.L. Prosser, Microtubules provide a viscoelastic resistance to myocyte motion, Biophys. J. 115 (9) (2018) 1796–1807, doi:10.1016/j.bpj.2018.09.019.
- [14] J.D. Stroud, C.F. Baicu, M.A. Barnes, F.G. Spinale, M.R. Zile, Viscoelastic properties of pressure overload hypertrophied myocardium: effect of serine protease treatment, 282 (6) (2002) 51-6, doi:10.1152/AJPHEART.00711.2001.
- [15] M.R. Zile, et al., Role of microtubules in the contractile dysfunction of hyper-trophied myocardium, J. Am. Coll. Cardiol. 33 (1) (1999) 250–260, doi:10.1016/S0735-1097(98)00550-6.
- [16] T.S. Harris, et al., Constitutive properties of hypertrophied myocardium: cellular contribution to changes in myocardial stiffness, Am. J. Physiol. Heart. Circ. Physiol. 282 (6) (2002), doi:10.1152/AJPHEART.00480.2001.
- [17] M.A. Caporizzo, C.Y. Chen, K. Bedi, K.B. Margulies, B.L. Prosser, Microtubules increase diastolic stiffness in failing human cardiomyocytes and myocardium, Circulation (2020) 902–915, doi:10.1161/CIRCULATIONAHA.119.043930.
- [18] H. Tsutsui, K. Ishihara, G. Cooper IV, Cytoskeletal role in the contractile dysfunction of hypertrophied myocardium, Science (1979) 260 (5108) (1993) 682–687, doi:10.1126/SCIENCE.8097594.
- [19] H. Tsutsui, et al., Role of microtubules in contractile dysfunction of hypertrophied cardiocytes, Circulation 90 (1) (1994) 533–555, doi:10.1161/01.CIR.90.1.
- [20] K.W. Prins, L. Tian, D. Wu, T. Thenappan, J.M. Metzger, S.L. Archer, Colchicine depolymerizes microtubules, increases junctophilin-2, and improves right ventricular function in experimental pulmonary arterial hypertension, J. Am. Heart. Assoc. 6 (6) (2017), doi:10.1161/JAHA.117.006195.
- [21] W. Liu, et al., Alterations of biaxial viscoelastic properties of the right ventricle in pulmonary hypertension development in rest and acute stress conditions, Front. Bioeng. Biotechnol. 11 (2023).
- [22] K.M. Labus, C.M. Puttlitz, Viscoelasticity of brain corpus callosum in biaxial tension, J. Mech. Phys. Solids. 96 (2016) 591–604, doi:10.1016/j.jmps.2016.08.

JID: ACTBIO ARTICLE IN PRESS [m5G;January 30, 2024;12:7]

K. LeBar, W. Liu, J. Pang et al.

Acta Biomaterialia xxx (xxxx) xxx

- [23] Y.C. Fung, Biomechanics: Mechanical Properties of Living Tissues, J. Appl. Mech. Eng. 49 (2) (1982) 464–465.
- [24] K. Roth, K. LeBar, W. Liu, M. Ahern, Z. Wang, Establishment of a biaxial testing system for characterization of right ventricle viscoelasticity under physiological loadings, Cardiovasc. Eng. Technol. (2023).
- [25] R.S. Lakes, Viscoelastic solids, Viscoelastic Solids (1998) 1–476, doi:10.1201/ 9781315121369.
- [26] B.G. Kerfant, G. Vassort, A.M. Gómez, Microtubule disruption by colchicine reversibly enhances calcium signaling in intact rat cardiac myocytes, Circ. Res. 88 (7) (2001). doi:10.1161/HH0701.090462.
- [27] W. Liu, et al., Multiscale contrasts between the right and left ventricle biomechanics in healthy adult sheep and translational implications, Front. Bioeng. Biotechnol. 10 (2022) 588, doi:10.3389/FBIOE.2022.857638/BIBTEX.
- [28] K. LeBar, W. Liu, A.J. Chicco, Z. Wang, Role of microtubule network in the passive anisotropic viscoelasticity of healthy right ventricle, Sci. Rep. (2023).
- [29] K.L. Troyer, C.M. Puttlitz, Human cervical spine ligaments exhibit fully nonlinear viscoelastic behavior, Acta Biomater. 7 (2) (2011) 700–709, doi:10.1016/J. ACTBIO.2010.09.003.
- [30] K.L. Troyer, D.J. Estep, C.M. Puttlitz, Viscoelastic effects during loading play an integral role in soft tissue mechanics, Acta Biomater. 8 (1) (2012) 234–243, doi:10.1016/J.ACTBIO.2011.07.035.

- [31] K.M. Labus, C.M. Puttlitz, Viscoelasticity of brain corpus callosum in biaxial tension, J. Mech. Phys. Solids. 96 (2016) 591–604, doi:10.1016/J.JMPS.2016.08. 010.
- [32] S. Dokos, B.H. Smaill, A.A. Young, I.J. LeGrice, Shear properties of passive ventricular myocardium, Heart Circulatory Physiol 283 (6) (2002) 2650–2659.
- [33] G. Cooper, Cytoskeletal networks and the regulation of cardiac contractility: microtubules, hypertrophy, and cardiac dysfunction, Heart Circulatory Physiol. 291 (3) (2006) 1003–1014.
- [34] Z. Wang, M.J. Golob, N.C. Chesler, Viscoelastic properties of cardiovascular tissues, Viscoelastic and Viscoplastic Materials, InTech, 2016, doi:10.5772/64169.
- [35] P. Robison, B.L. Prosser, Microtubule mechanics in the working myocyte, J. Physiol. 595 (12) (2017) 3931–3937.
- [36] Y.-H. Lin, et al., HDAC6 modulates myofibril stiffness and diastolic function of the heart, J. Clin. Invest. 132 (10) (2022).
- [37] A. R, H. MR, S. MA, Z. W, S. MS, A novel constitutive model for passive right ventricular myocardium: evidence for myofiber-collagen fiber mechanical coupling, Biomech. Model. Mechanobiol. 16 (2) (2017) 561–581, doi:10.1007/ S10237-016-0837-7.
- [38] D. Nordsletten, et al., A viscoelastic model for human myocardium, Acta Biomater. 135 (2021) 441–457.
- [39] S.S. Shetye, et al., Nonlinear viscoelastic characterization of the porcine spinal cord, Acta Biomater. 10 (2) (2014) 792–797, doi:10.1016/j.actbio.2013.10.038.